Shear induced structures of soft colloids: Rheo-SANS experiments on kinetically frozen PEP–PEO diblock copolymer micelles

2008 J. Phys.: Condens. Matter 20 404206

(http://iopscience.iop.org/0953-8984/20/40/404206)

J. Phys.: Condens. Matter **20** (2008) 404206 (9pp) doi:10.1088/0953-8984/20/40/404206

Shear induced structures of soft colloids: Rheo-SANS experiments on kinetically frozen PEP–PEO diblock copolymer micelles

J Stellbrink[1], **B Lonetti, G Rother, L Willner and D Richter**

Institut für Festkörperforschung Forschungszentrum Jülich, D-52425 Jülich, Germany

E-mail: j.stellbrink@fz-juelich.de

Received 1 May 2008, in final form 8 August 2008
Published 10 September 2008
Online at stacks.iop.org/JPhysCM/20/404206

Abstract

We investigated the effect of external steady shear on dilute to concentrated solutions of PEP–PEO diblock copolymer micelles (soft colloids). The degree of softness in terms of particle interactions (intermolecular softness) and deformability of the individual particle (intramolecular softness) was varied by changing the ratio between hydrophobic and hydrophilic blocks from symmetric (1:1, hard sphere-like) to very asymmetric (1:20, star-like).

We performed *in situ* rheology and small angle neutron scattering experiments (Rheo-SANS) to relate macroscopic flow properties to microscopic structural changes. The rheology data qualitatively show the same behavior for both types of micelles: (i) a divergence of the zero shear viscosity η_0 at a critical concentration ϕ_c approximately following a Vogel–Fulcher–Tammann law and (ii) close to this liquid–solid transition a shear rate dependent viscosity which can be described by the Carreau function with an asymptotic power law $\eta(\dot{\gamma}) \sim \dot{\gamma}^{-0.4}$ starting at a critical shear rate $\dot{\gamma}_c$.

Rheo-SANS experiments in the liquid phase close to ϕ_c were extended into the strong shear thinning region for both types of micelles at $\phi/\phi_c \approx 0.8$ and $\dot{\gamma}_{red} = \dot{\gamma}/\dot{\gamma}_c \approx 10$. In our Rheo-SANS data we observe a rather controversial influence of external shear on the structural properties of the two different micellar systems. With increasing shear rate the symmetric, hard sphere-like micelles show a decreasing structure factor $S(Q)$ but a shear rate independent interparticle distance. The asymmetric, star-like micelles show an increase in $S(Q)$ and an increase of the interparticle distance, both in the flow and vorticity direction. This unexpected behavior can be rationalized by a shear induced elongation and tilt of the star-like micelles along the flow direction as predicted by recent MD simulations (Ripoll *et al* 2006 *Phys. Rev. Lett.* **96** 188302).

(Some figures in this article are in colour only in the electronic version)

1. Introduction

In the last decade soft colloids have attracted the interest of the scientific community due to their hybrid nature. They share, at different length scales, the features of colloids and polymers and, as a consequence, they combine short range polymeric and long range colloidal interactions, which conveniently tuned can give rise to interesting and advantageous intermediate properties. The combination of complementary and even antagonistic interactions in order to design new technologically important structures constitute one of the main challenges in soft condensed matter [1].

Recently, concentration dependent gelation, vitrification or more general 'jamming' phenomena [2, 3] observed in dense solutions of soft colloids have attracted a lot of interest, due to their relevance for applications as well as for basic research.

[1] Author to whom any correspondence should be addressed.

Table 1. Molecular characteristics of PEP–PEO diblock copolymers.

Polymer	$M_{n,PEP}$[a] (g mol^{-1})	$d_{p,PEP}$[b]	$M_{n,PEO}$[c] (g mol^{-1})	$d_{p,PEO}$[b]	M_w/M_n[d]	Φ_{d-PEO}[e]
h-PEP4–dh-PEO4	4100	59	5 700	120	1.02	0.81
h-PEP1–hPEO20	1100	15	21 900	497	1.04	0.00

[a] ^{1}H-NMR.
[b] Degree of polymerization.
[c] Calculated.
[d] Overall polydispersity by GPC.
[e] Volume fraction deuterated EO.

In particular the observation of 'ageing' and 'rejuvenation' processes and questions of general 'history dependence', which crucially determine the flow properties of these systems have been intensively investigated [4, 5]. In this context also the question of 'yielding' [6, 7] or more generally 'what is still a fluid or already a solid' is controversially discussed. Experimentally most of these questions are investigated using rheological techniques. This discussion is directly linked to the question 'what is still an ergodic or already a non-ergodic system' often raised in the analysis of dynamic light scattering data [8]; in particular since the development of modern multi-speckle dynamic light scattering techniques extended the time window of conventional dynamic light scattering by some orders of magnitude [9–11]. The combination of rheology and dynamic light scattering as realized in a light scattering echo setup has also given fruitful new insights to this field of research [12, 13].

However, all these techniques are rather probing macroscopic to mesoscopic length and time scales in the range of 10^{-6}–10^{-3} m and 10^{-6}–10^{4} s. The link between macroscopic flow properties and microscopic structure can be set by performing *in situ* rheology and small angle neutron scattering experiments (Rheo-SANS) which resolve length scales from 10^{-9} to 10^{-6} m [14–16]. Also theoretically there have recently been important achievements in relating microscopic structure and macroscopic flow properties. Starting from mode coupling theory (MCT) Fuchs *et al* developed an approach [17, 18] that was recently confirmed by comparison with experiment [19, 20] for hard sphere systems.

We recently showed that micelles formed by the amphiphilic block copolymer poly(ethylene-alt-propylene)–poly(ethylene oxide) (PEP–PEO) provide an interesting system to conveniently tune the 'softness' in terms of particle interactions (intermolecular softness) and the deformability of the individual particle (intramolecular softness). This is achieved by changing the ratio between hydrophobic and hydrophilic blocks from symmetric (1:1, hard sphere-like) to very asymmetric (1:20, star-like) [21–24]. We must emphasize that to approach the star-like regime is not a trivial task. Preliminary SANS data, collected under steady shear, confirmed the expected crucial difference in sensitivity against the external perturbation [22]. With respect to preceding publication here we present a detailed rheological *in situ* characterization.

The paper is organized as follows. We start in section 2 with a brief summary of sample characteristics and equilibrium properties, which have been presented in detail in preceding publications [21–23], but which are the prerequisite for an understanding of the present work. Then we describe in detail the concept and design of the newly constructed Rheo-SANS setup. In section 3 first results obtained from Rheo-SANS experiments will be presented and discussed, starting with macroscopic flow properties before coming to the microscopic structural details resolved by the small angle neutron scattering experiments. Finally in section 4 we give some conclusions and an outlook for future experiments.

2. Experimental details

2.1. Synthesis

All polymers used in this study were prepared by anionic polymerization [25] and have been described in detail in [22, 26]. Numbers used for labeling different block copolymers denote the nominal molar volume, V_w, in dm^3 mol^{-1}, i.e. PEP4–PEO4 means a fully symmetric block copolymer where both the PEP and PEO block have the same molecular volume of ≈4000 cm^3 mol^{-1}. For completeness results from characterization by gel permeation chromatography (GPC), ^{1}H- and ^{13}C-NMR, are summarized in table 1. To fully exploit the capabilities of SANS experiments we made use of contrast variation/matching by preparing polymer solutions in mixtures of H_2O/D_2O, see section 2.3. The freeze dried polymer was dissolved in the appropriate solvent mixture, gently shaken for one hour at room temperature and heated to 60 °C for 3 h with repeated rapid mixing using a vortex mixer. Afterward samples were allowed to slowly cool down to room temperature over another 12 h. By strictly following this preparation protocol for all solutions under investigation we have been able to obtain reproducible results with respect to rheological and scattering properties.

2.2. Rheo-SANS setup

To perform *in situ* rheology and small angle neutron scattering (Rheo-SANS) we adapted a commercial strain controlled rheometer, Rheowis-Fluid (Labplus, Jona, Switzerland), to the special needs of a SANS experiment. For this reason we designed and constructed a Couette-type shear cell (concentric cylinders, outer cylinder rotating). We chose this particular geometry to fully decouple strain control and force

measurement. Shear cells are either made of sapphire or niobium which results in a neutron transmission of ≈88% and ≈80%, respectively. The outer cylinder (cup) has a diameter of 50 mm and a height of 80 mm. Using different inner cylinders (bobs) with either 49 or 48 mm diameter and 55 mm height we obtain corresponding gap widths of 0.5 and 1 mm (i.e. a total sample thickness for the neutron beam of 1 and 2 mm, respectively). Different to many other Rheo-SANS setups our cup and bob have been designed using a Mooney–Ewards geometry with a cone angle $\alpha = 21.1°$ to achieve high shear stability. Moreover, the rheometer is, in particular, optimized for high shear rates $\dot{\gamma}$ with a maximum of ≈10 000 s^{-1}. The force transducer covers a torque range from 1×10^{-7}–0.046 N m. In oscillatory shear the amplitude range is 5×10^{-2}–45° with a frequency range of 5×10^{-3}–10 s^{-1}. Temperature control is achieved by circulation of a thermostating fluid by a bath cryostat, Julabo F32ME (Julabo, Seelbach, Germany), to the cup from below and through a housing which covers the whole shear cell from above. This allows a temperature range of 5–90 °C with a precision of ±0.5 °C. The housing serves in addition as a solvent trap to avoid sample evaporation. The required sample volume is approximately 4.5–10 ml depending on gap width.

2.3. Rheo-SANS experiments

Rheo-SANS experiments were performed at the instruments KWS1 and KWS2 at Forschungszentrum Jülich, Jülich (Germany). We used neutron wavelengths of $\lambda = 6$ and 7 Å with a wavelength spread $\Delta\lambda/\lambda$ of 10% and 20%, respectively. Sample-to-detector distances and collimation lengths were set to D1.25C8(20), D2C8(20), D8C8(20) and D20C20 with a source aperture of 30 mm × 30 mm and a sample aperture of 10 mm × 10 mm. SANS data were corrected following standard procedures and normalized to absolute units (cm^{-1}) by a lupolen standard to allow a quantitative theoretical interpretation. During data analysis the experimental resolution function of the SANS instrument was taken into account [27]. For details concerning the experimental technique see for example [28]. All Rheo-SANS experiments were performed using radial geometry with a neutron beam passing through the center of the cylindrical shear cell, i.e. probing the flow and vorticity direction of the shear field. 2D analysis and model fitting of our SANS data was partly performed using the programs GRASP [29] and SASfit [30]. The macroscopic scattering cross section, $(d\Sigma/d\Omega)(Q)$, measured by SANS can be expressed as a product of single particle contributions, the particle form factor $P(Q)$, and the structure factor $S(Q)$, which contains all information about particle interactions:

$$\left(\frac{d\Sigma}{d\Omega}\right)(Q) = N_z\, P(Q)S(Q). \tag{1}$$

Here $Q = \frac{4\pi}{\lambda}\sin(\theta/2)$ is the scattering vector and N_z is the number density of particles. $S(Q)$ can be extracted from SANS data by dividing out $P(Q)$ measured in dilute solution. However, this procedure is only valid, if particle size and shape, i.e. $P(Q)$, are unaffected by concentration and/or external shear. This is in general not the case for deformable particles such as micelles. Moreover, following the approach of Kotlarchyk and Chen for polydisperse particles [31], it has been shown in recent studies that for block copolymer micelles the factorization of the scattering intensity into a form and structure factor following equation (1) in general does not hold due to lack of spherical symmetry of the micellar corona [32]. But we can overcome this problem by proper application of contrast variation techniques. The contrast in a neutron scattering experiment is given by the difference in scattering length densities between solute and solvent, which are calculated by

$$\rho_j = \frac{\sum b_i}{v_j} \tag{2}$$

with j the individual components PEP monomer, PEO monomer or solvent molecule, $\sum b_i$ the sum of the coherent scattering lengths of all atoms in component j, and v_j the average volume of one molecule of component j

$$v_j = \frac{M_j}{d_j N_A}. \tag{3}$$

M_j is the molar mass of the component j, and d_j its corresponding density. Performing all SANS experiments in core contrast, i.e. adjusting the scattering length density ρ_0 of the solvent by use of h/d-isotopic mixtures to that of PEO, reduces the contrast factor between corona and solvent to zero. Only the compact PEP core, which is completely unaffected by increasing concentration, is 'visible' in the SANS experiment. The quantitative analysis of SANS data obtained from micellar solutions of PEP–PEO diblock copolymers has been described in details in our previous publications so we refer the interested reader to the corresponding literature [21–24]. For completeness we summarize the previously obtained micellar characteristics for both types of micelles in table 2.

Table 2. Characterization of PEP–PEO block copolymer micelles in aqueous solution [22].

Polymer	N_{agg}	R_{core} (Å)	R_m [a] (Å)	R_{HS} [b] (Å)
h-PEP4–dh-PEO4	1600	145	280	290
h-PEP1–h-PEO20	122	40	299	0

[a] From micellar form $P(Q)$ at infinite dilution.
[b] From micellar structure factor $S(Q)$.

3. Results and discussion

Before presenting the response of $I(Q)$ to external shear we briefly summarize the rheological behavior of all samples under investigation. The shear rate dependence of the steady shear viscosity $\eta(\dot{\gamma})$ for all samples investigated in our Rheo-SANS experiments is presented in figure 1. Both dilute solutions show an almost full Newtonian behavior, i.e. a shear rate independent viscosity given by $\eta = \sigma/\dot{\gamma}$ (Newtonian plateau) with σ the measured shear stress. Only for PEP1–PEO20 is a small decrease of ≈8% observed at the highest shear rate. Both concentrated solutions show a clear dependence of η on shear rate (shear thinning). The viscosity

Table 3. Results from rheology.

Polymer	η_0 (Pa s)	$\dot{\gamma}_c$ (s^{-1})	b	ϕ_c (%)
h-PEP4–dh-PEO4[a]	0.050 ± 0.001	627 ± 19	0.61 ± 0.02	17.2 ± 0.02
h-PEP1–h-PEO20	0.042 ± 0.001	322 ± 45	0.58 ± 0.03	3.50 ± 0.01

[a] Only $500\ s^{-1} \leqslant \dot{\gamma} \leqslant 8000\ s^{-1}$.

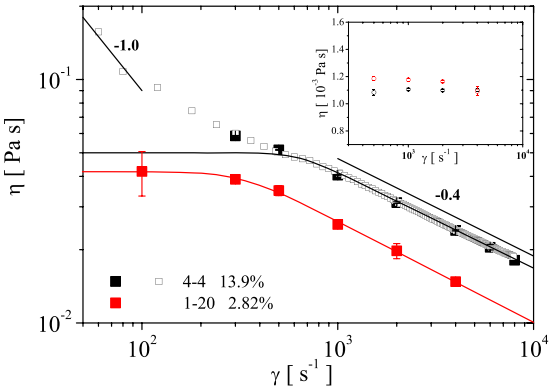

Figure 1. Experimental flow curves, i.e. viscosity η_0 versus shear rate $\dot{\gamma}$ for concentrated solutions of PEP–PEO micelles at $T = 20\,^{\circ}C$. Full symbols: mean values averaged over the duration of the Rheo-SANS experiment. Open symbols: flow curves measured directly before the Rheo-SANS experiment. Solid lines: fit to Carreau function (equation (4)), see the text. Inset: flow curves for corresponding dilute solutions.

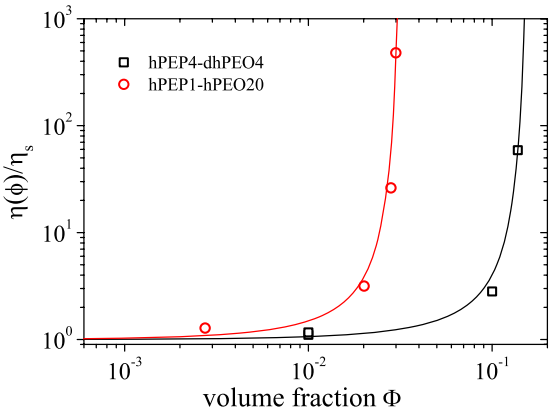

Figure 2. Concentration dependence of the reduced zero shear viscosity η/η_s versus shear rate $\dot{\gamma}$ at $T = 20\,^{\circ}C$ (for hPEP4-dhPEO4 the value from the small Newtonian plateau observed for $\dot{\gamma} \approx 500\ s^{-1}$ is shown for $\phi = 13.9\%$). Solid lines: fit to VFT function (equation (5)), see the text.

of the star-like micellar solution formed by PEP1–PEO20 at a volume fraction $\phi = 2.82\%$ starts with a Newtonian plateau before a power law like decay, $\eta \sim \dot{\gamma}^{-0.4}$, sets in. In contrary the viscosity of the hard sphere-like micellar solution formed by PEP4–PEO4 at $\phi = 13.9\%$ shows no Newtonian plateau but directly starts with a power law decay, $\eta \sim \dot{\gamma}^{-1}$, already at the smallest experimental shear rate. Such a different behavior is expected since PEP1–PEO20 at $\phi = 2.82\%$ is well within the liquid phase, whereas PEP4–PEO4 at $\phi = 13.9\%$ is already in the 2-phase region of coexisting liquid and crystal phase. Only at intermediate shear rates, $\dot{\gamma} \approx 500\ s^{-1}$, a small region of constant viscosity is found. With further increasing shear rate a second power law regime starts, but now with approximately the same exponent, $\eta \sim \dot{\gamma}^{-0.4}$, as observed for the star-like micelles. At the highest experimental shear rate a reduction of the viscosity by a factor of $0.042/0.015 \approx 0.5$ and $0.059/0.019 \approx 0.3$ is obtained for PEP1–PEO20 and PEP4–PEO4, respectively. A power law dependence $\eta \sim \dot{\gamma}^{-0.5}$ is often experimentally observed for soft colloids [33], whereas the steeper decay $\eta \sim \dot{\gamma}^{-1}$ is typical of a strong shear thinning solid. The observation of such a decay in the first points for PEP4–PEO4 at $\phi = 13.9\%$ indicates that this sample is already close to complete freezing as expected for hard sphere-like colloids at this volume fraction.

There exist several models in literature for describing a shear rate dependent viscosity. Often applied for soft colloids are the empirical Cross and the Carreau equations [34, 35], the latter one is given by:

$$\eta(\dot{\gamma}) = \frac{\eta_0}{[1 + (\dot{\gamma}/\dot{\gamma}_c)^a]^{\frac{1-b}{a}}}. \qquad (4)$$

Here η_0 denotes the zero shear viscosity, $\dot{\gamma}_c$ indicates the onset of the shear thinning and has the dimensions of s^{-1}; the power law exponent, $(1 - b)$, describes the dependence of the viscosity on shear rate in the shear thinning region and the additional dimensionless parameter a represents the width of the transition region between the constant Newtonian plateau observed at low shear rates and the asymptotic power law decrease of the viscosity found at high shear rates. Commonly values equal to 2 are observed. The use of a Carreau function compares to the use of a Kohlrausch–Williams–Watts function, i.e. a 'stretched' exponential decay, instead of a single exponential decay in the analysis of dynamic light scattering data [36]. The obtained fits of the Carreau equation for both concentrated solutions are also shown in figure 1 and agree reasonably with our experimental data. We must point out that for the symmetric PEP4–PEO4 we only analyzed the region $\dot{\gamma} \geqslant 500\ s^{-1}$ due to the presence of the steeper initial decay. All obtained parameters are summarized in table 3. Whereas the critical shear rate, $\dot{\gamma}_c$, differs by a factor of ≈ 2, both micellar systems show approximately the same zero shear viscosity $\eta_0 \approx 0.05$ Pa s and the same power law exponent $(1 - b) \approx 0.4$. We emphasize, that the obtained value for the reduced viscosity $\eta_{red} = \eta_0/\eta_{solv}$ for the symmetric PEP4–PEO4 gives a value of $\eta_{red} = 50$, with $\eta_{solv} = 1$ mPa s^{-1}, the viscosity of the solvent. This value agrees nicely with the previously reported value of 53 ± 6 for a hard sphere system at freezing [37].

The critical shear rate, $\dot{\gamma}_c$, corresponds to the minimum shear rate that perturbs the system, which in turn is the inverse of its characteristic relaxation time τ_c. Taking the obtained values from the fit, $\dot{\gamma}_c = 627\ s^{-1}$ for PEP4–PEO4 and

$\dot{\gamma}_c = 322\ s^{-1}$ for PEP1–PEO20, we obtain characteristic relaxation times in the millisecond range, i.e. $\tau_c = 1.6$ ms and $\tau_c = 3.1$ ms, respectively.

For PEP1–PEO20 we also performed dynamic light scattering and pfg-^{1}H-NMR experiments from which we derived a value of $1.34 \times 10^{-13}\ m^2\ s^{-1}$ for the self diffusion coefficient D_{self} at $\phi = 2.82\%$ [38]. Therefore we can compare the time τ needed for a single star-like micelle to diffuse over the mean intermicellar distance $D = \frac{2\pi}{Q_m}$ given by the peak position Q_m from SANS, see section 2.3, to the characteristic time obtained from the fitting of the Carreau equation (4). With $D = 2\pi/1.073 \times 10^{-2}\ Å^{-1} = 586$ Å we obtain $\tau = 4.3$ ms which reasonably agrees with $\tau_c = 3.1$ ms obtained from rheology and consistently confirms our experimental results. Due to the strong turbidity of PEP4–PEO4 solutions we were not able to perform dynamic light scattering experiments for the other micellar system.

The power law exponents indicate the dependence of the shear viscosity on the shear rate and for fluids they are usually between 0.3 and 0.5 [39], while higher values are expected for more structured liquids characterized by longer relaxation times [40]. For example, a value of 0.67 was found by Holmes *et al* in the case of a 122 arm star polymer solution in decane slightly above the overlap concentration c^* where the sample is defined as a very weak gel [41]. Nicolai *et al* report a value of 0.83 in the case of a 20% volume fraction solution of Brij700, a PEO end-capped with an octadecyl chain forming micelles with aggregation number $N_{agg} = 42$ [42, 43].

Obtaining good counting statistics in a Rheo-SANS experiment often requires measurement times of the order of several hours, in particular at large sample-to-detector distances. Therefore the question of sample ageing arises, in particular for concentrated solutions. To check this we performed some selected experiments in a twofold manner. Most experiments were done with an abrupt increase from zero shear (equilibrium) to the required value of $\dot{\gamma}$, which was then hold constant for the remaining time of the SANS experiment. During this period the shear stress σ (or viscosity η) was measured in different time intervals so that up to 250 individual data points were collected during one single Rheo-SANS experiment. For almost all samples the value of σ was constant to within 5–10% during the whole experimental time. The filled symbols in figure 1 denote the mean values obtained from all individual data points measured at a given shear rate. In addition for some selected samples we started with a shear rate ramp from zero to the required value of $\dot{\gamma}$ over a period of 5–15 min, before this was held constant and the SANS data acquisition was started. Such a flow curve (or rate sweep) is also shown in figure 1 as open symbols for PEP4–PEO4 at $\phi = 13.9\%$. Obviously there is no difference between the results of both types of experiments, clearly indicating that we are still in a concentration range where ageing is not relevant.

The concentration dependence of the reduced zero shear viscosity $\eta_{red} = \eta_0(\phi)/\eta_{solv.}$ is shown in figure 2. For both types of micelles we observe a strong increase of η_{red} with increasing volume fraction ϕ giving some evidence for a divergence at a certain critical volume fraction ϕ_c, which crucially depends on the system. We tried to parameterize both

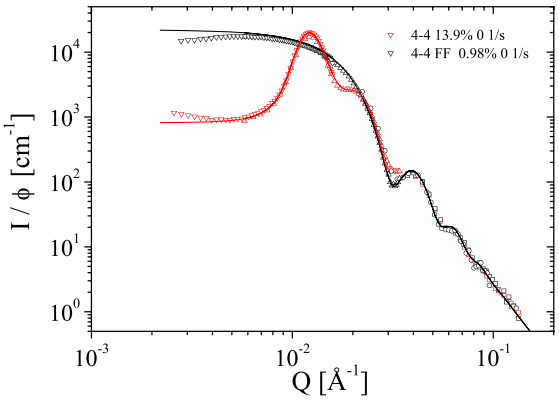

Figure 3. SANS intensity $I(Q)$ versus scattering vector Q data without shear for PEP4–PEO4, $\phi = 13.9\%$ and 0.98% without shear at $T = 20\,°C$. Solid line: form factor obtained from the preceding publication [22] and calculated hard sphere structure factor [30].

data sets by fitting our experimental data to a Vogel–Fulcher–Tammann-like behavior (VFT):

$$\eta_0(\phi) \sim \exp -\frac{1}{(\frac{\phi}{\phi_c} - 1)} \tag{5}$$

from which we determined the following values of $\phi_c = 17.2\%$ for PEP4–PEO4 (hard sphere-like) and $\phi_c = 3.5\%$ for PEP1–PEO20 (star-like). Using ϕ_c we can calculate a reduced volume fraction $\phi_{red} = \phi/\phi_c$ to define the distance to the observed liquid–solid transition. The concentrated solutions for both types of micelles under investigation have approximately the same value $\phi_{red} \approx 0.8$.

Figure 3 shows the corresponding SANS data without external shear for the hard sphere-like micelles formed by PEP4–PEO4. The calculated form factor $P(Q)$ extrapolated to infinite dilution using the parameters from a preceding study [22] given in table 2 is also shown as a solid line in figure 3. For the higher concentration, $\phi = 13.9\%$, i.e. $\phi_{red} = 0.81$, a strong structure factor peak is clearly visible, but also for the rather moderate concentration, $\phi = 0.98\%$ i.e. $\phi_{red} = 0.06$, a clear reduction of the forward scattering $I(Q = 0)$ is found compared to the form factor. Also shown in figure 3 is the calculated intensity for hard spheres using the decoupling approach for form and structure factor proposed by Kotlarchyk and Chen [31]. Again we have to emphasize that this is not a fit, we just used the previously determined parameters to calculate $I(Q)$ [22]. The hard sphere volume fraction $\phi_{hs} = \frac{4\pi}{3} R_{hs}^3 N_z$ is calculated from the given number density of micelles $N_z = \frac{\phi\, d\, N_A}{M_w N_{agg}}$ and the corresponding hard sphere radius R_{hs}, which gives $\phi_{hs} \approx 0.53$. In figure 4 the corresponding SANS data without shear of micelles formed by the asymmetric PEP1–PEO20 are shown for a dilute, $\phi = 0.27\%$, i.e. $\phi_{red} = 0.08$ and a concentrated solution, $\phi = 2.82\%$, i.e. $\phi_{red} = 0.81$. We must point out that, contrary to the preceding publication [22], for this system we used full contrast, i.e. fully protonated polymers in D_2O, in order to see the effect of external shear on the diffuse micellar corona. This is indicated by the appearance of the asymptotic power law $I \sim Q^{-5/3}$ at high Q-vectors for both concentrations, which results from the so called 'blob'

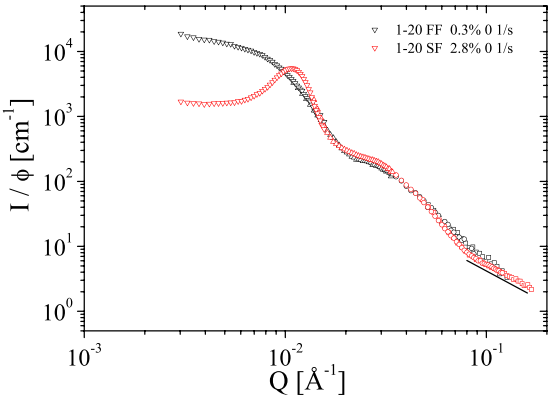

Figure 4. SANS intensity $I(Q)$ versus scattering vector Q data without shear for hPEP1-hPEO20, $\phi = 2.82\%$ and 0.27% in D_2O without shear at $T = 20\,^{\circ}C$. Solid line: expected power law from 'blob' scattering $\sim Q^{-5/3}$, see the text [22].

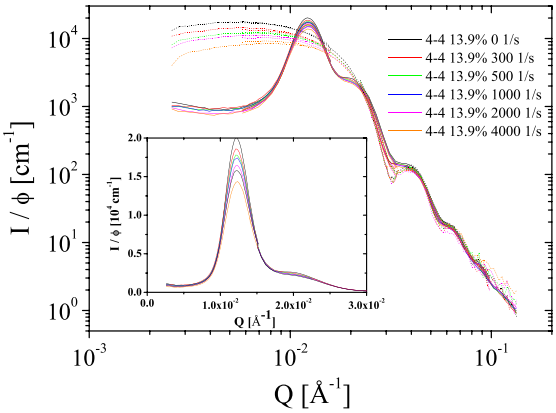

Figure 6. SANS data for PEP4–PEO4, $\phi = 13.9\%$ (solid lines) and $\phi = 0.98\%$ (dotted lines) in core contrast ($\phi_{D_2O} = 0.92$) at $T = 20\,^{\circ}C$ at different shear rates. Inset: zoom of the Q-region around the first structure factor peak for $\phi = 13.9\%$.

scattering [32]. Therefore in the present paper we are not able to simply derive an experimental structure factor by use of the factorization given in equation (1) (see also the discussion in section 2.3). So we have to discuss $I(Q)$ instead, however, also for the concentrated solution of star-like micelles a strong structure factor peak is directly visible in $I(Q)$, reflecting its vicinity to the liquid–solid transition, see the discussion above.

The effect of external shear on the microscopic structure of the hard sphere-like system PEP4–PEO4 becomes directly visible in figure 5, which shows the two-dimensional SANS data at $\phi = 13.9\%$, i.e. $\phi_{red} = 0.81$, without and with external shear. The typical Debye–Scherrer ring indicating a liquid-like structure observed without external shear clearly develops some precursors of Bragg reflections when moderate shear, $\dot{\gamma} = 300\ s^{-1}$, is applied. We only observe four reflections in our 2D data instead of six as expected for a fcc lattice. This effect can be attributed to the shear field which decreases the intensities of the two inner nodes on the vorticity axis [14]. But with a further increase of shear rate these Bragg reflections disappear and eventually up to the highest experimentally accessible shear rate only Debye–Scherrer rings are again observed. This behavior indicates that our sample is close to a fluid–crystal phase transition as already concluded from our rheological data: first shear induced crystallization takes place but the formed (weak) crystal can easily be shear melted by further increasing the shear rate.

For the concentrated sample of PEP1–PEO20 (star-like micelles), on the other hand, no evidence for a shear induced crystallization is found in our 2D SANS data. In the following we therefore only present one-dimensional, radially averaged data, i.e. $I(Q)$ in absolute units (cm^{-1}) versus scattering vector Q.

Again, we will start with PEP4–PEO4 (hard sphere-like micelles). Data from Rheo-SANS experiments extending deep into the shear thinning regime are shown in figure 6 for concentrations $\phi = 0.98\%$ (dilute) and $\phi = 13.9\%$ ($\phi_{red} = 0.81$, i.e. close to fluid–solid phase transition). Already for the dilute sample with $\phi = 0.98\%$ the effect of external shear is clearly visible. With increasing shear rate $\dot{\gamma}$ a reduction of forward scattering, i.e. an increase in compressibility of the system, occurs. One has to note that at this concentration a fully Newtonian behavior is observed at all shear rates. The viscosity $\eta(\dot{\gamma})$ measured *in situ* during the SANS experiment is constant within 1%, $\bar{\eta} = 1.10 \pm 0.01$ mPa s, see the inset of figure 1. For the concentrated solution of PEP4–PEO4 the effect of reduced forward scattering is less pronounced, but

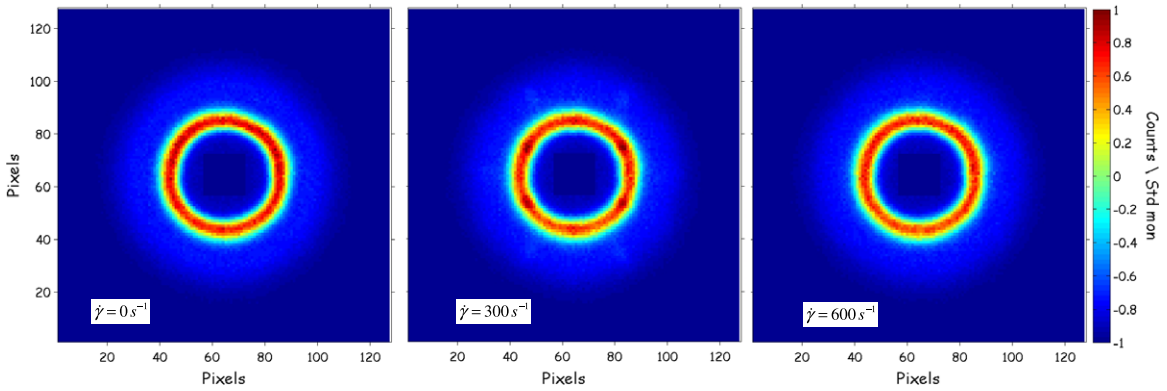

Figure 5. 2D SANS data for PEP4–PEO4, $\phi = 13.9\%$, corresponding to $\phi_{hs} = 0.53$, at different shear rates $\dot{\gamma}$ at $T = 20\,^{\circ}C$. With increasing shear rate $\dot{\gamma}$ precursors of Bragg reflections can be seen, which disappear upon a further increase of $\dot{\gamma}$.

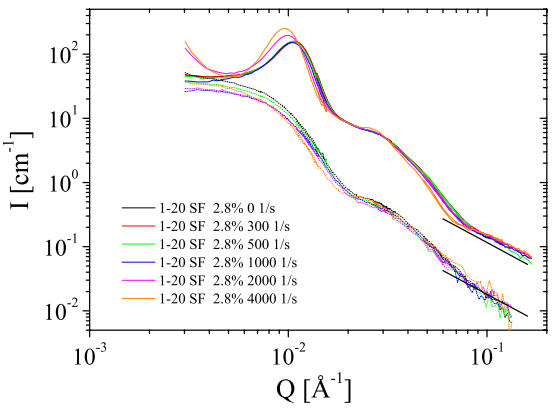

Figure 7. SANS data for PEP1–PEO20, $\phi = 2.82\%$ (solid lines) and $\phi = 0.27\%$ (dotted lines) in full contrast ($\phi_{D_2O} = 1.0$) at $T = 20\,^{\circ}$C at different shear rates.

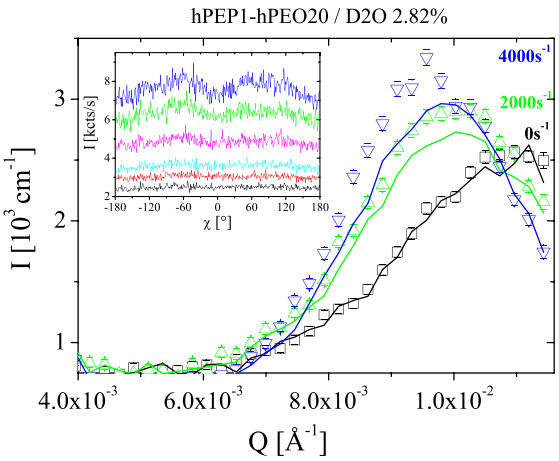

Figure 8. Intensity $I(Q)$ versus scattering vector Q from anisotropic analysis of SANS data for PEP1–PEO20, $\phi = 2.82\%$ at different shear rates in full contrast ($\phi_{D_2O} = 1.0$), $T = 20\,^{\circ}$C. Symbols: flow direction, lines: vorticity direction. With increasing shear rate the data for flow and vorticity direction split, both showing a shift of the peak position Q_m to lower Q-vectors. Inset: intensity versus radial scattering angle χ at peak position Q_m showing an increasing anisotropy with increasing shear rate. For clarity data are shifted by a multiplicative factor: $\dot{\gamma} = 0{:}1$, $\dot{\gamma} = 300{:}1.25$, $\dot{\gamma} = 500{:}1.5$, $\dot{\gamma} = 1000{:}2$, $\dot{\gamma} = 2000{:}2.25$ and $\dot{\gamma} = 4000{:}2.5$ (from bottom to top).

in addition the height of the first peak in the structure factor continuously decreases with increasing shear rate, see the inset of figure 6. In addition, the peak position Q_m is completely unchanged at all shear rates, even in the strong shear thinning regime up to $\dot{\gamma}_{red} = \dot{\gamma}/\dot{\gamma}_c \approx 10$. This means that the typical interparticle distance $D \approx \frac{2\pi}{Q_m}$ remains constant at a value of about 517 Å. Another estimate for the mean interparticle distance is obtained from $N_z^{-1/3}$, which gives 569 Å, which has to be related to the hard sphere and micellar radius of PEP4–PEO4 micelles, $R_{hs} = 290$ Å and $R_m = 280$ Å. All numbers corroborate the very high packing fraction of the sample with $\phi = 13.9\%$.

Compared to our previous results on the same system [22] we now observe a continuous decrease in $S(Q)$ with increasing shear rate. This can be rationalized by the higher quality of the present data in particular for the high shear rates due to the special design of the newly developed shear cell. In general, our results are comparable to experiments performed by Johnson *et al* [16] on solutions of sterically stabilized silica spheres. These authors found qualitatively the same effects and analyzed their data in terms of theories developed by Ronis [44] and Dhont [45]. However, these theories neglect the influence of hydrodynamic interactions, which might explain the need for an arbitrary shift factor to match experiment and theory [16]. We can conclude that our micelles also behave as hard spheres under the influence of external shear.

In figure 7 the corresponding Rheo-SANS data for star-like micelles formed by the asymmetric PEP1–PEO20 are shown (for clarity reasons we do not use the presentation $I(Q)/\phi$ as used in figure 6, but rather $I(Q)$). Whereas for the dilute solution of star-like micelles qualitatively the same effects are observed as for the hard sphere-like micelles, for the concentrated solution at $\phi = 2.82\%$, i.e. $\phi_{red} = 0.81$, a completely different effect of external shear is found. Striking is the strong influence on the Q-dependence, which was completely absent for the hard sphere-like micelles. For PEP1–PEO20 a shift of the first structure factor peak to lower Q-vectors occurs, indicating an increase of the interparticle distance. Also a strong increase of the forward scattering $I(Q = 0)$ is observed at the two highest shear rates $\dot{\gamma} = 2000\ s^{-1}$ and $\dot{\gamma} = 4000\ s^{-1}$. The typical interparticle distance $D \approx \frac{2\pi}{Q_m}$ for PEP1–PEO20 changes with increasing shear from 578 to 657 Å, i.e. by ≈12%. Recently multiparticle collision dynamics simulations (MPC) [46] have predicted a shear induced deformation of regular star polymers, the limiting ultra-soft colloid [47]. These simulations show an elongation of star polymers with increasing shear rate along the flow direction in line with a decrease along the gradient and vorticity direction. Due to the applied full contrast condition we are not able to separate shear effects on form and structure factor in our present SANS experiments. Although no anisotropy is directly seen in the 2D SANS data for PEP1–PEO20, we nevertheless performed a more careful analysis in the Q-range around the structure factor peak Q_m to check for any indication of shear induced anisotropy. Only for the data with the highest Q-resolution, i.e. those taken at the longest sample-to-detector distance D20C20, did we find some evidence. For this reason we plotted (i) the intensity distribution $I(\chi)$ at a fixed scattering angle θ (corresponding to a fixed Q-vector Q_m) along the azimuthal angle $-180^{\circ} \leqslant \chi \leqslant +180^{\circ}$, i.e. within a ring on the 2D detector area and (ii) the full Q-dependence along flow and vorticity direction by averaging along two orthogonal strips at $\chi = 0$ and 90. The results from this kind of analysis are shown in figure 8. First, with increasing shear rate a deviation from $I(\chi) = \text{const}$ is observed giving a clear evidence for structural anisotropy, see the inset of figure 8. Even more obvious is the effect of shear when we compare the data along flow (symbols) and vorticity direction (lines). Whereas at rest, $\dot{\gamma} = 0$, data for both directions fall on top of each other as expected for an isotropic system, with increasing shear $I(Q)$ along flow and vorticity split, but show qualitatively the same behavior: an

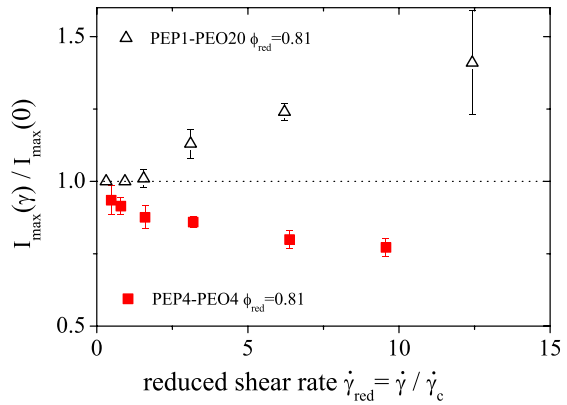

Figure 9. Reduced height of first structure factor peak, $I_{red} = I(\dot{\gamma})/I(0)$, versus reduced shear rate, $\dot{\gamma}_{red} = \dot{\gamma}/\dot{\gamma}_c$, for PEP4–PEO4, $\phi = 13.9\%$, and PEP1–PEO20, $\phi = 2.82\%$, both at $\phi_{red} = \phi/\phi_c = 0.81$ and $T = 20\,^{\circ}$C.

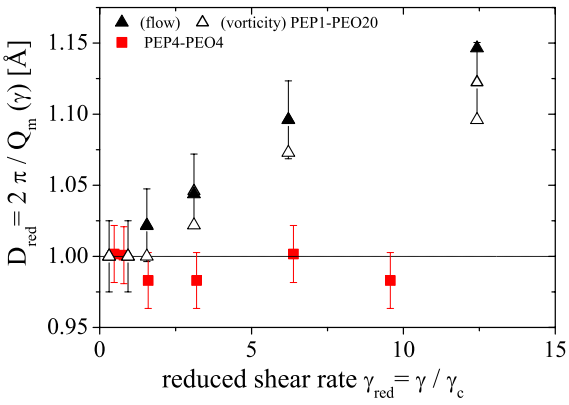

Figure 10. Reduced interparticle distance from position Q_m of the first structure factor peak, $D_{red} = D(\dot{\gamma})/D(0)$, versus reduced shear rate, $\dot{\gamma}_{red} = \dot{\gamma}/\dot{\gamma}_c$, for PEP4–PEO4, $\phi = 13.9\%$ (squares), and PEP1–PEO20 (closed triangles: flow direction, open triangles: vorticity direction), $\phi = 2.82\%$, both at $\phi_{red} = \phi/\phi_c = 0.81$ and $T = 20\,^{\circ}$C.

increase in peak height $I(Q)$ and a shift of the peak position to lower Q-vectors. Both effects are more pronounced along the flow direction, i.e. a ≈15% increase/shift along the flow and ≈10% increase/shift along the vorticity direction. The effect along the flow direction can be intuitively rationalized: at rest, for this concentrated solution the micelles are close to contact since $D = \frac{2\pi}{Q_m} \approx 2R_m$. If a shear induced deformation occurs, i.e. an elongation along the flow direction as predicted by simulation, there are now two possibilities for the system to adapt for the new situation: (i) either the micellar coronas have to overlap more strongly, while keeping the distance between two micelles along the flow direction constant, or (ii) the micelles separate to avoid this energetically unfavorable overlap. At the same time one might expect that in the perpendicular (vorticity) direction the mean intermicellar distance is decreasing but we observe exactly the opposite in our experiments. This unexpected result can also be explained in terms of the simulation results. Ripoll *et al* predict a tilt angle of the elongated star polymers with respect to the flow direction and a tank treading motion of the star polymer arms around the star center [46]. Therefore, also along the vorticity direction the 'mean size' of the deformed particle as seen by its neighbors increases, which in turn causes an increase of the interparticle distance also along the vorticity direction as observed by the shift of the peak position to lower Q-vectors. The effect of external shear on concentrated solution for both micellar systems is finally summarized in figure 9. Here the reduced height of the first structure factor peak, $I_{red} = I(\dot{\gamma})/I(\dot{\gamma} = 0)$, is shown as a function of the reduced shear rate, $\dot{\gamma}_{red} = \dot{\gamma}/\dot{\gamma}_c$. Whereas for the hard sphere-like micelles of PEP4–PEO4 this values continuously decreases with increasing shear, for the star-like micelles of PEP1–PEO20 exactly the opposite trend occurs. The same presentation is used for the reduced intermicellar distance obtained from the position of the first structure factor peak, $D_{red} = D(\dot{\gamma})/D(\dot{\gamma} = 0) = Q_m(\dot{\gamma} = 0)/Q_m(D\dot{\gamma})$ shown in figure 10. Whereas for the hard sphere-like micelles of PEP4–PEO4 this values remains constant with increasing shear, for the star-like micelles of PEP1–PEO20 there is an continuous increase of D_{red}, along both the flow and vorticity directions, as already discussed above.

Finally, at the highest shear rate, $\dot{\gamma} = 4000\ s^{-1}$, a small second order peak or shoulder appears in the radially averaged data for PEP1–PEO20 shown in figure 7 around $Q \approx 2.5 \times 10^{-2}$ Å^{-1}. The ratio between the position of the second and first peak is of the order of ≈7, which cannot be ascribed to some simple crystal structure. In addition, in the region $3 \times 10^{-2} \leqslant Q \leqslant 8 \times 10^{-2}$, a clear shift of the decay of the scattering intensity to smaller Q-vectors is visible, again indicating a growing length scale with increasing shear. A proper decomposition into form and structure factor contributions is not possible under the present contrast conditions: In this Q-region both, the scattering from the micellar corona and the micellar core mix with structure factor effects, but probably zero-average contrast experiments would help for elucidating this observation.

4. Conclusions

Rheo-SANS experiments are an excellent tool to relate macroscopic flow properties to the microscopic structure in sheared colloidal solutions. We investigated soft colloids with varying degrees of softness close to their liquid–solid transition, which was determined by the concentration dependence of the zero shear viscosity η_0. For both systems the shear rate dependence of $\eta(\dot{\gamma})$ shows a strong shear thinning behavior following an asymptotic power law dependence $\sim\dot{\gamma}^{-0.4}$. The full shear rate dependence can be described by a Carreau function, from which a critical shear rate $\dot{\gamma}_c$ is determined, which gives the onset of the shear thinning region. Rheo-SANS experiments were performed both in the Newtonian regime as well as in the strong shear thinning limit up to values of $\dot{\gamma}/\dot{\gamma}_c \approx 10$. Whereas the symmetric, hard sphere-like micelles show a decreasing structure factor $S(Q)$ with increasing shear rate but a shear rate independent interparticle distance, the asymmetric, star-like micelles show

both an increase in $S(Q)$ and an increase of the interparticle distance with increasing shear rate. Unexpectedly this increase of about ≈10–15% occurs along both the flow and vorticity directions, which can be rationalized by an elongation of the micelles together with a tilt with respect to the flow lines, as predicted by recent MD simulations [46].

Acknowledgments

We acknowledge G Petekidis and D Vlassopoulos for helpful discussions and the Deutsche Forschungsgemeinschaft (DFG) for financial support in the framework of the Transregio Sonderforschungsbereich TR6 (Teilprojekt A2).

References

[1] Muthukumar M, Ober M and Thomas E L 1997 *Science* **277** 1225
[2] Liu A J and Nagel S R 1998 *Nature* **396** 21
[3] Trappe V, Prasad V, Cipelletti L, Segre P N and Weitz D A 2001 *Nature* **411** 772
[4] Purnomo E H, van den Ende D, Mellema J and Mugele F 2006 *Europhys. Lett.* **76** 74
[5] Mazoyer S, Cipelletti L and Ramos L 2006 *Phys. Rev. Lett.* **97** 238301
[6] Rogers S A, Vlassopoulos D and Callaghan P T 2008 *Phys. Rev. Lett.* **100** 128304
[7] Smith P A, Petekidis G, Egelhaaf S U and Poon W C K 2007 *Phys. Rev.* E **76** 041402
[8] Pusey P N and Van Megen W 1989 *Physica* A **157** 705
[9] Kirsch S, Frenz V, Schartl W, Bartsch E and Sillescu H 1996 *J. Chem. Phys.* **104** 1758
[10] Cipelletti L, Bissig H, Trappe V, Ballesta P and Mazoyer S 2003 *J. Phys.: Condens. Matter* **15** S257
[11] Scheffold F and Cerbino R 2007 *Curr. Opin. Colloid Interface Sci.* **12** 50
[12] Hébraud P, Lequeux F, Munch J P and Pine D J 1997 *Phys. Rev. Lett.* **78** 4657
[13] Petekidis G, Moussaid A and Pusey P N 2002 *Phys. Rev.* E **66** 051402
[14] Vermant J and Solomon M J 2005 *J. Phys.: Condens. Matter* **17** R187
[15] Förster S, Timmann A, Schellbach C, Fromsdorf A, Kornowski A, Weller H, Roth S V and Lindner P 2007 *Nat. Mater.* **6** 888
[16] Johnson S J, de Kruif C G and May R P 1988 *J. Chem. Phys.* **89** 5009
[17] Fuchs M and Cates M E 2002 *Phys. Rev. Lett.* **89** 248304
[18] Fuchs M and Cates M E 2003 *Faraday Discuss.* **123** 267
[19] Fuchs M and Ballauf M 2005 *J. Chem. Phys.* **122** 094707
[20] Crassous J, Siebenbürger M, Ballauff M, Drechsler M, Henrich O and Fuchs M 2006 *J. Chem. Phys.* **125** 204906
[21] Lund R, Willner L, Stellbrink J, Radulescu A and Richter D 2004 *Macromolecules* **37** 9984
[22] Stellbrink J, Rother G, Laurati M, Lund R, Willner L and Richter D 2004 *J. Phys.: Condens. Matter* **16** S3821
[23] Laurati M, Stellbrink J, Lund R, Willner L, Richter D and Zaccharelli E 2005 *Phys. Rev. Lett.* **94** 195504
[24] Laurati M, Stellbrink J, Lund R, Willner L, Richter D and Zaccharelli E 2007 *Phys. Rev.* E **76** 041503
[25] Hsieh H L and Quirk R P 1994 *Anionic Polymerisation* (New York: Dekker)
[26] Poppe A, Willner L, Allgaier J, Stellbrink J and Richter D 1997 *Macromolecules* **30** 7462
[27] Pedersen J S, Posselt D and Mortensen K 1990 *J. Appl. Crystallogr.* **23** 321
[28] Higgins J S and Benoit H C 1994 *Polymers and Neutron Scattering* (Oxford: Oxford University Press)
[29] Dewhurst C 2003 *GRASP User Manual* (Grenoble: ILL)
[30] Kohlbrecher J, Buitenhuis J, Meier J and Lettinga M P 2006 *J. Chem. Phys.* **125** 044715
[31] Kotlarchyk M and Chen S H 1983 *J. Chem. Phys.* **79** 2461
[32] Pedersen J S 2001 *J. Chem. Phys.* **114** 2839
[33] Senff H and Richtering W 1999 *J. Chem. Phys.* **111** 1705
[34] Cross M M 1965 *J. Colloid Sci.* **20** 417
[35] Carreau P J 1972 *Trans. Soc. Rheol.* **16** 99
[36] Patterson G D and Lindsey C P 1980 *J. Chem. Phys.* **73** 3348
[37] Meeker S P, Poon W C K and Pusey P N 1997 *Phys. Rev.* E **55** 5718
[38] Stellbrink J 2008 in preparation
[39] Bird R B, Armstrong R C and Hassager O 1987 *Dynamics of Polymeric Liquids* 2nd edn, vol 1 (New York: Wiley)
[40] Rabin Y and Ottinger H C 1990 *Europhys. Lett.* **13** 413
[41] Holmes W M, Callaghan P T, Vlassopoulos D and Roovers J 1998 *J. Rheol.* **48** 1085
[42] Lafiche F, Nicolai T and Durand D 2003 *Macromolecules* **36** 1341
[43] Nicolai T and Benyahia L 2005 *Macromolecules* **38** 9794
[44] Ronis D 1984 *Phys. Rev.* A **29** 1453
[45] Dhont J K G 1989 *J. Fluid Mech.* **204** 421
[46] Ripoll M, Winkler R G and Gompper G 2006 *Phys. Rev. Lett.* **96** 188302
[47] Likos C N, Watzlawek M, Löwen H, Abbas A, Jucknischke O, Allgaier J and Richter D 1998 *Phys. Rev. Lett.* **80** 4450